CrystEngComm

Cite this: *CrystEngComm*, 2012, **14**, 8097–8102

www.rsc.org/crystengcomm

PAPER

Constrained growth of anisotropic magnetic δ-FeOOH nanoparticles in the presence of humic substances†

A. Yu. Polyakov,[a] A. E. Goldt,[a] T. A. Sorkina,[b] I. V. Perminova,[b] D. A. Pankratov,[b] E. A. Goodilin*[ab] and Y. D. Tretyakov[ab]

Received 4th June 2012, Accepted 29th August 2012
DOI: 10.1039/c2ce25886b

Natural polyelectrolytes, humic substances, are suggested to control *in situ* growth of feroxyhyte nanoparticles of a highly reduced mean size and with enhanced colloidal stability in salt solutions. The feroxyhyte is formed as 2–5 nm thick and 20 × 20 nm wide nanoflakes due to the blocking of developing facets of feroxyhyte and constraints caused by diffusion limitations of ionic constituents across partially charged branches of humic substances.

Introduction

Superparamagnetic iron oxide nanoparticles (SPIONs) are known as effective biocompatible agents for various biomedical applications like drug delivery, *in vivo* magnetic resonance imaging, cell and protein separation, hyperthermia and transfection.[1–8] At present, synthesis and application of rods, disks, fibers, tubes, sheets, ellipsoids, dumbbell-shaped, acorn-shaped and other anisotropic nanoparticles attract growing attention because of their unique properties.[2–6] Aggregation is a serious problem in the preparation and storage of such magnetic nanoparticles limiting considerably their practical applications. This problem can be solved by a surface modification of nanoparticles with organic macromolecules, their preparation in the presence of surfactants, application of hydrophilic, surface-active ligands[9-11] improving biocompatibility[12–14] and resulting in multifunctional nanoparticles for medical diagnostics.[15,16]

Contrary to other ferrimagnetic iron oxides, feroxyhyte can be formed under mild conditions[17–19] and therefore has a large amount of surface hydroxyl groups readily available for targeted modifications. Moreover, feroxyhyte possesses a layered structure, a high specific surface area and pronounced adsorption properties.[20] This compound is used as a sorbent for removal of toxic ions from wastewater,[21,22] a precursor for high coercivity materials,[23,24] and as a photocatalyst for water splitting.[25] Feroxyhyte also is a participant of complex processes of organic–inorganic interactions in biogeochemical systems. The striking example is crystallinity control that natural organic matter imposes over amorphous iron hydroxides in soils and deep sea sediments leading to formation of extremely disperse feroxyhyte.[17,18] While soil scientists see a template role of organic matter in this process serving as a crystallization inhibitor, the marine researchers explain it by degradation of organic matter which yields reducing conditions necessary for releasing iron ions from sedimentary minerals or clays.

The former mentioned global processes underline a unique synthetic niche of humic substances (HS) in SPION and other nanomaterial transformation processes.[26–28] Indeed, humic substances are believed to be a new candidate for the size and morphology control of SPIONs; they are essentially a complex mixture of natural macromolecular compounds with vast functional peripheries dominated by carboxyl and hydroxyl groups. They possess properties of anionic polyelectrolytes and reveal a distinct affinity for surface complexation of SPIONs.[29] Perhaps they can bind nanoparticles both by electrostatic surface interactions and iron chelation. At least, it is highly possible that HS interact with iron oxides and stabilize them in the form of multinuclear hydroxy complexes or nanoparticles in their soils.[30,31] In the present work we investigate humic substances as a new cheap and effective "green" stabilizer for feroxyhyte magnetic nanoparticles. We report a direct experimental evidence of the template role of this natural organic matter in the synthesis of δ-FeOOH. The results deepen our understanding of regulatory drivers in the organic–inorganic systems that may be used for improving iron bioavailability as well as for development of new classes of SPIONs for nanomedicine.

Experimental

High-purity $FeCl_2 \cdot 4H_2O$ was purchased from ABCR GmbH&Co (Germany). Potassium humate was purchased from "Sakhalinsky Humates" (groups of companies, Russia). According to manufacturer's information, potassium humate was produced by alkaline extraction from leonardite. Iron content in the humate did not exceed 1 wt% according to

[a]*Department of Materials Science, Moscow State University, Lenin Hills, Moscow, 119991, Russia. E-mail: goodilin@gmail.com; Tel: +7495 9394609*
[b]*Chemistry Department, Moscow State University, Lenin Hills, Moscow, 119991, Russia*
† Electronic supplementary information (ESI) available. See DOI: 10.1039/c2ce25886b

chemical analysis data. All other reagents were of analytical grade. All solutions were prepared using de-ionized water.

A series of feroxyhyte nanoparticles was synthesized by oxidizing of 0.1 M $FeCl_2$ solutions with H_2O_2 (30%) at pH 8 in the presence of 100 mg L^{-1} of humic substances (HS) or without it. HS were added into the reaction mixture in a form of alkaline solution (pH 12) which was prepared by dissolution of dry samples of potassium humate in alkali under ultrasonic treatment for 30 min. Thus total deprotonation of carboxylic and phenolic groups of HS was achieved and these groups became activated for stabilization of iron oxide nanoparticles. The obtained concentrated suspensions of organic–inorganic composites (δ-FeOOH-HS) were separated from a supernatant by centrifugation (10 000 rpm, 5 min) and then dried in a vacuum oven at room temperature.

X-ray powder diffraction (XRD) data for all the samples were collected in a step scan mode at room temperature using Rigaku D/Max 2500 diffractometer with a rotating anode (Cu-Kα radiation, θ–2θ Bragg–Brentano geometry, 25–70° range, 0.02° step). For phase identification, the ICDD PDF2 database[32] was used. Peak positions as well as peak half-widths were elucidated using Le Bail technique[33] implemented in the Jana2006 software.[34]

Particle morphologies and microstructures were observed by transmission electron microscopy (TEM, LEO912 AB OMEGA). Mean particle sizes were estimated using the data of typically 200+ particles taken from TEM images.

Mössbauer absorption spectra were recorded using a MS1104EM express Mössbauer spectrometer (MosTek, Rostov-on-Don) with ^{57}Co in a rhodium matrix as the radiation source, activity 3.5 and 10 mCi (Cyclotron, Obninsk), in the 5–298 K temperature range. Chemical shifts were measured using α-Fe as a standard. Temperature was maintained within ±1 K. The spectra were fitted using the least-squares minimization procedure by standard programs.

Magnetic properties were analyzed using a Faraday balance magnetometer in the field range of −10 000 to 10 000 Oe at room temperature.

All size distribution and zeta potential measurements were performed using a Malvern Zetasizer Nano ZS instrument at 25 °C at scattering angle (175°) and detection angle (12.8°) with a He–Ne laser (laser power 4 mW, wavelength 632.8 nm and beam diameter 0.63 mm). The samples were placed in standard Malvern zeta potential disposable capillary cells and polystyrene cuvettes for zeta potential and size measurements, respectively. To estimate colloidal stability, pristine magnetic nanoparticles or those stabilized with humic substances were held in a physiological salt solution (normal saline, 0.9% of NaCl) for 9 days with intermediate particle size measurements by DLS.

Results and discussion

All the synthesized products demonstrate main XRD peaks corresponding to δ-FeOOH (ICDD PDF2 entry #13-87, Fig. 1). Estimated cell parameters (Table 1) corroborate well the results reported elsewhere.[35] The positions of two broad bumps between 2θ = 25–40° and 2θ = 55–60° are close to those of the most intense hematite peaks; the appearance of hematite phase was also described.[36] The peak half-widths indicate strong anisotropic broadening of (101) reflections being much more severe in

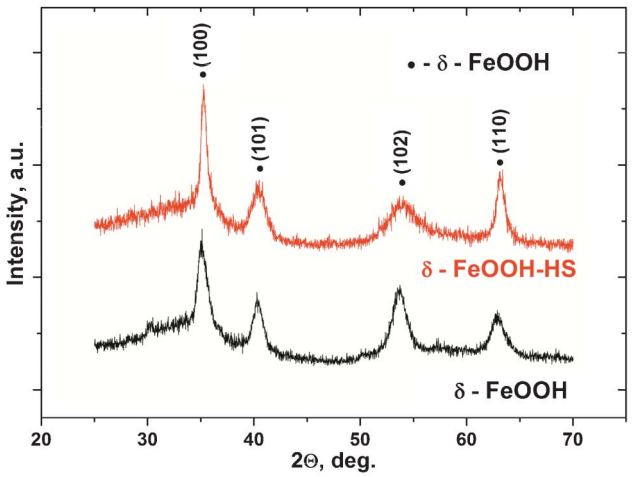

Fig. 1 X-ray patterns of δ-FeOOH phases. The lower curve corresponds to pure δ-FeOOH while the upper one represents δ-FeOOH obtained in the presence of HS.

the case of HS-synthesized δ-FeOOH. Since the (001) direction corresponds to interlayer stacking, we can suppose that the main source of broadening is caused by narrowing of δ-FeOOH particles in this direction indicative of a platelet shape of diffracting domains and their smaller size in the case of HS-prepared nanoparticles.

Morphology features of the δ-FeOOH particles determined by TEM (Fig. 2) reveal that both pure δ-FeOOH and magnetic nanocomposites of δ-FeOOH with HS can be described as nanoflakes with a mean size along the largest axis of about 160 nm and 20 nm and the thickness 20 nm and 2 nm, respectively. The microphotograph (Fig. 2a) shows that the shape of the δ-FeOOH plates is irregular and the size distribution of the particles is broad, whereas in the case of nanoparticles stabilized by HS (Fig. 2b), the size distribution seems to be narrower (Fig. 2d) with the aspect ratio of about 9–10 in both cases. Therefore it is evident that the size is drastically changed in the presence of HS while the growth anisotropy remains almost same.

A closer view reveals that nanoparticles in the composite are partly stacked (Fig. 2c) which could be associated with their entrapment into HS. It is known that HS of the selected molecular weight typically demonstrate a hydrodynamic diameter of about 100–200 nm in aqueous solution.[26] Such a large space allocated in the solution to HS makes it possible to incorporate more than one SPION per molecule of HS. When considering the ratios and concentration of reagents and geometric sizes of HS-stabilized SPIONs, it could be estimated that one feroxyhyte nanoparticle is accompanied with an excess of 1.5–2 molecules of HS. Therefore, it might be suggested that

Table 1 Measurements of FWHM of peaks and unit cell parameters of δ-FeOOH

	Unit cell parameters		FWHM, deg			
Sample	*a*/Å	*c*/Å	(100)	(101)	(102)	(110)
δ-FeOOH	2.954(1)	4.600(2)	0.96(7)	1.08(7)	1.40(9)	1.66(9)
δ-FeOOH-HS	2.947(1)	4.583(6)	0.59(4)	1.52(9)	2.17(9)	0.82(5)

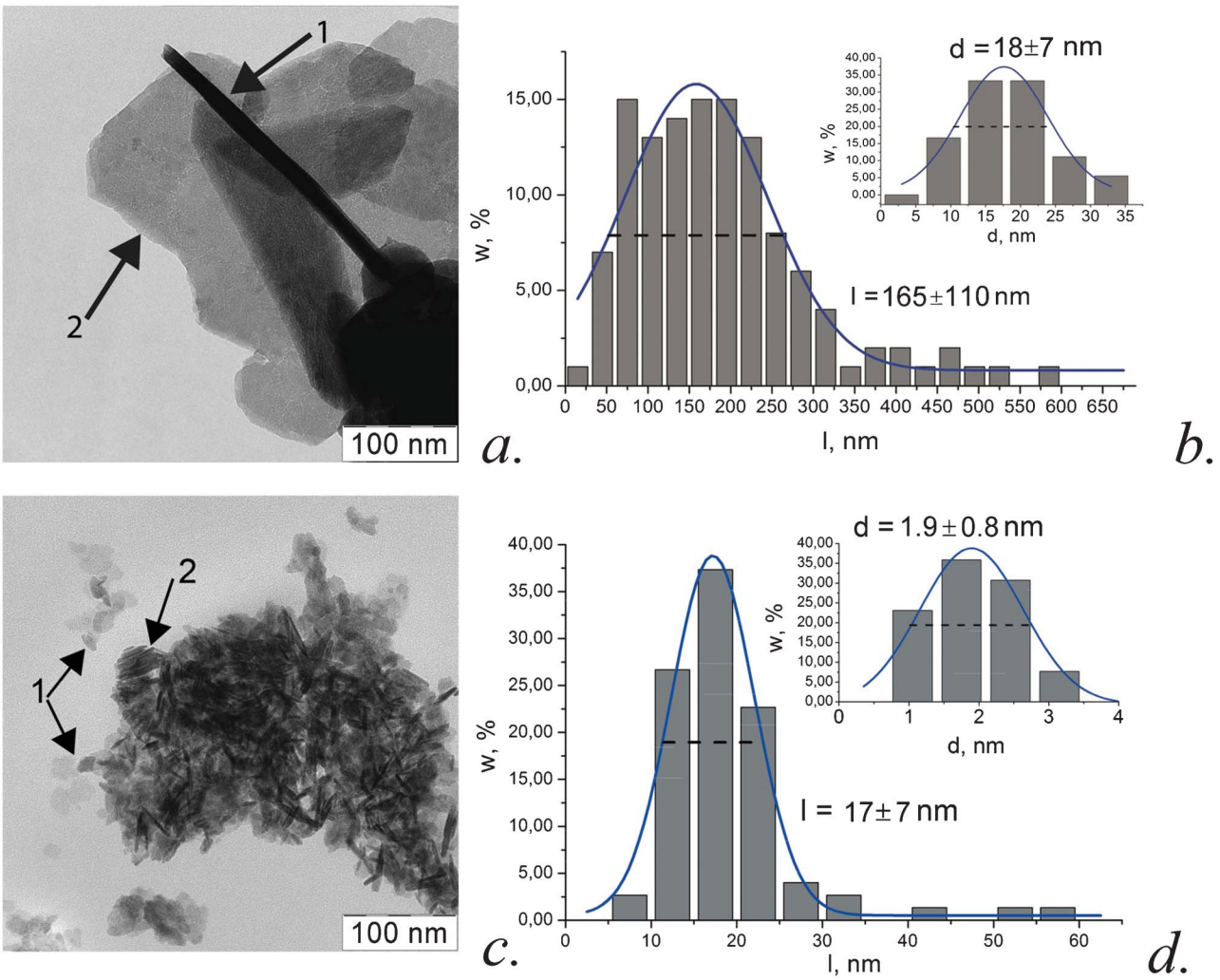

Fig. 2 TEM micrographs and size distributions (sizes along the largest axis, "*l*", and thickness, "*d*") for pure δ-FeOOH (a, b) and the composite δ-FeOOH-HS (c, d). 1, δ-FeOOH nanoflakes lying perpendicularly to the view; 2, in-plane δ-FeOOH nanoflakes.

HS remove nuclei or embryocrystals of SPIONs from the colloidal solution due to a high affinity to them.

It is worth mentioning that the embryocrystals are represented by tiny nanoparticles of $Fe(OH)_2$ formed at the first stage of addition of alkali into the $FeCl_2$ solution to achieve pH 8 in the reaction mixture. These $Fe(OH)_2$ nanocrystals are entrapped into the HS "matrix" and $Fe(OH)_2$-HS conglomerates are formed. At the same time, formation of $Fe(OH)_2$ nuclei outside the HS branched structure is not affected and this process develops multiple embryocrystals prepared for embedding into HS. The $Fe(OH)_2$-HS conglomerates operate as growth domains in the reaction mixture, however additional Fe^{2+} and OH^- ions diffusing into the limited volume of the domain became distributed among several embryocrystals in the $Fe(OH)_2$-HS conglomerates (Fig. 3). Such an ion transport would be also affected by a partial negative charge of the HS branches catching cations and repelling anions. These factors lead to slower growth of $Fe(OH)_2$ particles of the domain in comparison with non-embedded embryocrystals.

It should be also noted that electrode potentials of HS varies from +0.33 to +0.70 V,[29] being close enough to that of the Fe(III)/Fe(II) pair under standard conditions. However such a protection of $Fe(OH)_2$ from oxidation with oxygen becomes impossible at experimental pH values. Further rapid oxidation of $Fe(OH)_2$ into feroxyhyte using 30% H_2O_2 plays a significant role in the controlled growth of δ-FeOOH nanoparticles. The

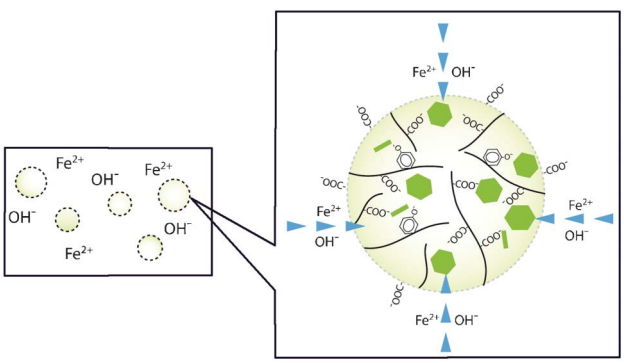

Fig. 3 A model of nanoparticle constrained growth in the presence of humic substances.

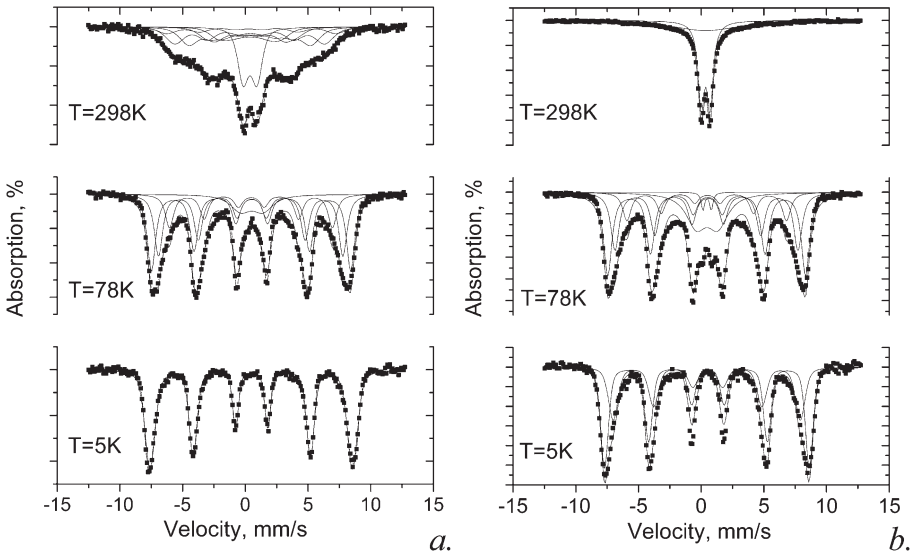

Fig. 4 Mössbauer spectra at different temperatures of the pure δ-FeOOH (a) and composite δ-FeOOH-HS (b).

oxidation is accomplished in a few seconds and neither particle growth nor structural rearrangement may occur for this period of time; δ-FeOOH phase, which is isostructural to $Fe(OH)_2$, forms. Feroxyhyte nanoparticles remain embedded into the HS matrix and therefore have almost the same morphology and small size as the initial $Fe(OH)_2$ embryocrystals.

The nanoparticles possess distinct magnetic properties as shown in Fig. 4 and 5. The room temperature magnetic hysteresis loops (Fig. 5) revealed that the coercivity is about 250 Oe at 300 K for pure δ-FeOOH and 70 Oe for the δ-FeOOH-HS composite. These results are in a good agreement with the difference in particle sizes as found by TEM (Fig. 2) and with the decrease of iron concentration in the composite because of the presence of HS. Indeed, δ-FeOOH nanoparticles embedded into the HS matrix are smaller than a single domain size for iron oxides and this makes the nanoparticles superparamagnetic, although their inability to rotate freely guarantees a small coercitivity. HS-free feroxyhyte plates are of drastically enlarged size which provides a higher coercive force.

The above results corroborate well the findings of Mössbauer spectroscopy on the superparamagnetic nature of the particles (Fig. 4). The latter allows for an investigation of nanocrystalline δ-FeOOH embedded into HS since Mössbauer spectroscopy is known to be sensitive to both magnetic behaviour of SPIONs and superficial states of the probe iron atoms. These features seem to be essential in the case of ultradisperse particles of SPIONs.

The Mössbauer spectrum of pure δ-FeOOH in Fig. 4a shows a substantial broadening at 295 K, typical for magnetic nanoparticles with fluctuations of the magnetization direction; this spectrum seems to be a combination of FM (ferromagnetic) and SPM (superparamagnetic) components. The FM part of the spectrum is the majority (80% area), it is represented in total by unresolved sextets (components A1–A5, Table 2). The spectral shape suggests that the magnetic fluctuations are influenced by interparticle interactions in their polydispersed ensemble. At liquid nitrogen temperature, such a spectrum might be described by a superposition of sextets (components B1–B3, Table 2, Fig. 4a). The blocking temperature of the δ-FeOOH sample is rather high, which is why the paramagnetic part vanishes. Indeed, in the low-temperature spectrum obtained at 5 K, there are no indications of any "paramagnetic" components. This shows that Fe^{3+} ions are present in the bulk of magnetically ordered δ-FeOOH phase.

The Mössbauer spectra of the composite demonstrated a superparamagnetic behaviour as shown in Fig. 4b. At 298 K, 62% of the spectrum is a doublet with an isomer shift of 0.36 mm s^{-1} and quadrupole splitting of 0.71 mm s^{-1} corresponding to the SPM state (component D1, Table 2).

The difference is evidently relayed on a lower blocking temperature due to much smaller particle sizes of the HS-stabilized sample. The FM part of the spectrum is unresolved and could be ascribed with a broad resonance line. The isomer shift of 0.37 mm s^{-1} of the component D1 (Table 2) corresponds well to the same parameter of the paramagnetic doublet. With lowering temperature, the paramagnetic signals from Fe^{3+} ions

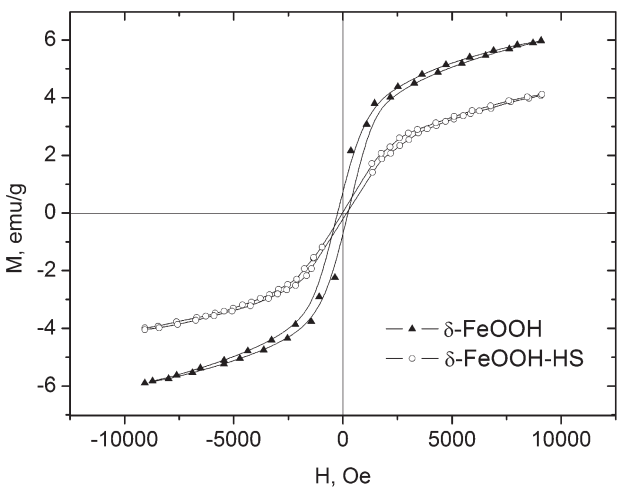

Fig. 5 Magnetization curves for the powders of δ-FeOOH-HS composite and δ-FeOOH at 300 K.

Table 2 Hyperfine parameters of the pure δ-FeOOH and δ-FeOOH nanoparticles stabilized with HS (δ +/− 0.01 mm s^{-1}, isomer shift relative to α-Fe; Δ +/− 0.01 mm s^{-1}, quadrupole splitting or shift; Γ_{exp}, the full line width at half height; H_{in} +/− 0.1 kOe, internal magnetic field (kOe))

Sample/temperature	Component	δ mm s^{-1}	Δ	Γ_{exp}	H_{in} kOe	Area fraction (%)
δ-FeOOH 298 K	A1	0.37	0.22	1.74	418.7	9
	A2		−0.05		370.5	21
	A3		−0.03		301.2	23
	A4		0.13		212.2	14
	A5		−0.07		153.9	13
	A6	0.37	1.09	1.01		20
δ-FeOOH 78 K	B1	0.48	−0.05	0.79	493.4	40
	B2	0.47	−0.08		456.6	33
	B3	0.46	−0.03		403.4	18
	B4	0.51	1.79	1.94		9
δ-FeOOH 5 K	C1	0.49	−0.04	0.75	501.3	100
δ-FeOOH-HS 298 K	D1	0.36	0.71	0.59		62
	D2	0.37		6.63		38
δ-FeOOH-HS 78 K	E1	0.48	−0.09	0.79	490.0	40
	E2	0.47	−0.06		453.1	28
	E3	0.47	−0.06		394.9	13
	E4	0.47	1.73	1.94		17
	E5	0.47	0.66	0.32		2
δ-FeOOH-HS 5 K	F1	0.50	0.08	0.73	507.1	60
	F2	0.48	−0.08	0.91	463.3	40

at 298 K turn into sets of hyperfine structure lines (HFS) reflecting the presence of δ-FeOOH nanoparticles in a magnetically ordered state (components E1–E3, Table 2). At liquid nitrogen temperature, the HS-stabilized sample with smaller particles shows lower internal magnetic field values (490.0, 453.1, 394.9 kOe) for probe iron atoms in comparison with the ones of HS-free sample (493.4, 456.6, 403.4 kOe). In addition, small doublets (components E4–E5, Table 2) are present in the spectrum owing to the residual SPM state because of a lower blocking temperature.

Liquid helium temperatures result in complete magnetic ordering of both the samples (Fig. 4a, 4b). However, there is an additional essential feature observed for the HS-stabilized sample related to the presence of an extra sextet appearing in the spectrum (component F2, Table 2). It can be estimated from the TEM data that only 10% of iron atoms are superficial for the HS-free sample, while this ratio reaches 50% for the smaller HS-stabilized particles. It seems that coordination of those superficial atoms is strongly influenced by binding to HS. As a result, the subspectrum F1 with the larger magnetic field value still corresponds to the bulk atoms, while another subspectrum F2 represents superficial probe atoms with peculiar HS coordination (Fig. 4b, Table 2).

This interaction of the magnetic nanoparticles with humic substances is also evident from their enhanced colloidal stability in the presence of HS as shown in Fig. 6. Bare nanoparticles precipitate quickly after a couple of days since they aggregate immediately in the salt solution forming objects with large radii exceeding 700 nm. Light fractions of 100–200 nm survive for additional three days and then the solution becomes gradually clean. A quite different situation is observed for the HS-stabilized magnetic nanoparticles. They form 200–250 nm composite particles containing branched humic substances and multiple magnetic nanoparticles.[26] They are stabilized either sterically, because of the branch architecture of HS, or electrostatically, since HS are charged, for at least 9 days with no radius changes or precipitation observed.

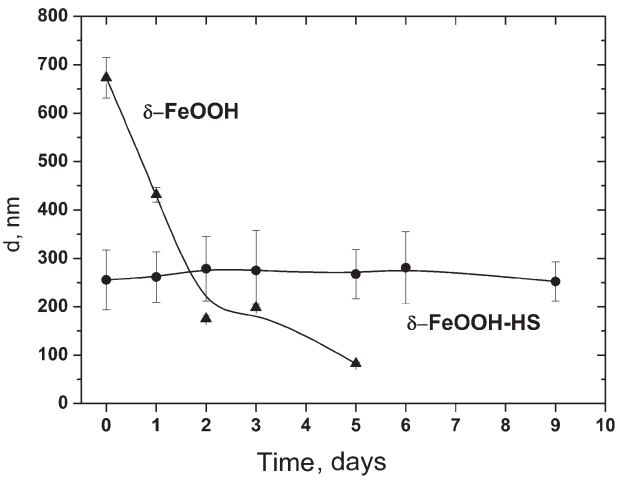

Fig. 6 DLS data on estimated hydrodynamic radii of pristine feroxyhyte nanoparticles and those stabilized *in situ* with humic substances in NaCl saline solution.

Thus humic substances applied *in situ* in the process of nanoparticle preparation play a dual role allowing the achievement of a much smaller size for the nanoparticles and allow the nanoparticle be stable in water solutions. The latter and know biocompatibility of such composite nanoparticles[8,26] (see also ESI†) suggests to us that the new preparation technique is suitable for nanomedicine purposes.

Conclusions

An application of humic substances is found to result in reduction of a medium particle size of δ-FeOOH for at least one order of magnitude. The feroxyhyte nanoparticles reveal their high crystallographic anisotropy by forming nanoflakes possessing 2–5 nm thickness and 20 × 20 nm in-plane size. The influence of humic acids in the control of δ-FeOOH particle size

seems to relate to both blocking of developing facets and producing constraints for fast diffusion of ionic constituents needed for fast growth due to a high molecular weight nature and partial charges of humic acid branches. The results deepen our understanding of regulatory drivers in the organic–inorganic systems that may be used for improving iron bioavailability as well as for development of new classes of SPIONs for nanomedicine.

Acknowledgements

The authors are thankful to *RFBR* No. 10-03-00976-a, *RFBR* No. 11-03-00761-a, 11-03-12177 and the Development Program of MSU. The authors thank to Eduard Levin, Sergey Kushnir, Lev Trusov and Alexey Garshev for their help and discussions.

References

1 Y. Gossuin, P. Gillis, A. Hocq, Q. L. Vuong and A. Roch, *Wiley Interdiscip. Rev.: Nanomed. Nanobiotechnol.*, 2009, **1**, 299–310.
2 E. Hao, G. C. Schatz and J. T. Hupp, *J. Fluoresc.*, 2004, **14**, 331–341.
3 K. J. Lee, J. Yoon and J. Lahann, *Curr. Opin. Colloid Interface Sci.*, 2011, **16**, 195–202.
4 J.-W. Yoo, N. Doshi and S. Mitragorti, *Macromol. Rapid Commun.*, 2010, **31**, 142–148.
5 I. V. Roslyakov, K. S. Napol'skii, A. A. Eliseev, A. V. Lukashin, D. Yu. Chernyshov and S. V. Grigor'ev, *Nanotechnol. Russ.*, 2009, **4**, 176–181.
6 D.-H. Kim, *et al.*, *Nat. Mater.*, 2009, **9**, 165–171.
7 M. Raileanu, M. Crisan, C. Petrache, D. Crisan and M. Zaharescu, *J. Optoelectron. Adv. Mater.*, 2003, **5**, 693–698.
8 Q. A. Pankhurst, *Hyperfine Interact.*, 1994, **90**, 201–214.
9 A. Hajdu, E. Illes, E. Tombacz and I. Borbath, *Colloids Surf., A*, 2009, **347**, 104–108.
10 J. Park, M. K. Yu, Y. Y. Jeong, J. W. Kim, K. Lee, V. N. Phan and S. Jon, *J. Mater. Chem.*, 2009, **19**, 6412–6417.
11 A. K. Gupta and M. Gupta, *Biomaterials*, 2005, **26**, 3995–4021.
12 M. Mahmoudi, A. Simchi, H. Vali, M. Imani, M. A. Shokrgozar, K. Azadmanesh and F. Azari, *Adv. Eng. Mater.*, 2009, **11**, B243–B250.
13 M. K. Yu, J. Park, Y. Y. Jeong, W. K. Moon and S. Jon, *Nanotechnology*, 2010, **21**, 415102.
14 M. K. Yu, Y. Y. Jeong, J. Park, S. Park, J. W. Kim, J. J. Min, K. Kim and S. Jon, *Angew. Chem., Int. Ed.*, 2008, **47**, 5362–5365.
15 X. Yang, S. Pilla, J. J. Grailer, D. A. Steeber, S. Gong, Y. Chend and G. Chend, *J. Mater. Chem.*, 2009, **19**, 5812–5817.
16 D. Patel, A. Kell, B. Simard, J. Deng, B. Xiang, H.-Y. Lin, M. Gruwel and G. Tian, *Biomaterials*, 2010, **31**, 2866–2873.
17 U. Schwertmann, *Nature*, 1966, **212**, 645–646.
18 L. Carlson and U. Schwertmann, *Clays Clay Miner.*, 1980, **28**(4), 272–280.
19 U. Schwertmann and R. M. Cornell, *Iron Oxides in the Laboratory*, WILEY-VCH, Weinheim, 2000.
20 R. M. Cornell and U. Schwertmann, *The Iron Oxides: Structure, Properties, Reactions, Occurrences and Uses*, WILEY-VCH, Weinheim, 2003.
21 J. Hu, I. M. C. Lo and G. Chen, *Sep. Purif. Technol.*, 2007, **58**, 76–82.
22 K. Müller, V. S. T. Ciminelli, M. S. S. Dantas and S. Willscher, *Water Res.*, 2010, **44**, 5660–5672.
23 C. Tsung-Shune, D. Ming-Cheng and H. Sung-Lin, *Mater. Chem. Phys.*, 1994, **37**, 45–51.
24 S. Hao, X. Wang, Y. Wei, Y. Wang and C. Liu, *Rare Met.*, 2006, **25**, 466–470.
25 M. C. Pereira, *et al.*, *J. Mater. Chem.*, 2011, **21**, 10280–10282.
26 A. E. Chekanova, T. A. Sorkina, V. N. Nikiforov, G. A. Davidova, I. I. Selezneva, E. A. Goodilin, A. L. Dubov, L. A. Trusov, V .V. Korolev, I. M. Aref'ev, I. V. Perminova and Y. D. Tretyakov, *Mendeleev Commun.*, 2009, **19**, 72–74.
27 V. L. Pallem, H. A. Stretz and M. J. M. Wells, *Environ. Sci. Technol.*, 2009, **43**, 7531–7535.
28 R. Baigorri, J. M. García-Mina, R. F. Aroca and R. A. Alvarez-Puebla, *Chem. Mater.*, 2008, **20**, 1516–1521.
29 M. H. B. Hayes, P. MacCarthy, R. L. Malcolm and R. S. Swift, *Humic Substances II: In Search of Structure*. Wiley-Interscience, New York, 1989.
30 D. P. E. Dickson and I. Rozenson, *J. Phys. Colloq.*, 1980, **41**, C1-409.
31 A. Perez-Sanz and M. C. Graham, *Chemosphere*, 2006, **65**, 2045–2053.
32 ICDD PDF2 database, http://www.icdd.com/products/pdf2.htm.
33 A. Le Bail, H. Duroy and J. L. Fourquet, *Mater. Res. Bull.*, 1988, **23**, 447–452.
34 V. Petricek, M. Dusek and L. Palatinus, *Jana2006, The crystallographic computing system*, Institute of Physics, Praha, Czech Republic, 2006.
35 L. Carlson and U. Schwertmann, *Clays Clay Miner.*, 1980, **28**, 272–280.
36 V. A. Drits, B. A. Sakharov and A. Manceau, *Clays Clay Miner.*, 1993, **28**, 209–222.

